Journal of Advanced Ceramics
2016, **5**(3): 262–268
DOI: 10.1007/s40145-016-0198-9

ISSN 2226-4108
CN 10-1154/TQ

Research Article

Heat generation properties in AC magnetic field for composite powder material of the $Y_3Fe_5O_{12}$–*n*SiC system prepared by reverse coprecipitation method

Hiromichi AONO[a,*], Yuhi YAMANO[a], Takashi NAOHARA[a], Yoshiteru ITAGAKI[a], Tsunehiro MAEHARA[a], Hideyuki HIRAZAWA[b]

[a]*Graduate School of Science and Engineering, Ehime University, Matsuyama 790-8577, Japan*
[b]*National Institute of Technology, Niihama College, Niihama 792-8580, Japan*

Received: April 02, 2016; Revised: May 30, 2016; Accepted: June 17, 2016

Abstract: Composite powder material of the $Y_3Fe_5O_{12}$–*n*SiC system was synthesized by a reverse coprecipitation method to study its heat generation property in an AC magnetic field. For $Y_3Fe_5O_{12}$ ($n = 0$), the maximum heat generation ability of 0.45 $W \cdot g^{-1}$ in an AC magnetic field (370 kHz, 1.77 $kA \cdot m^{-1}$) was obtained for the sample calcined at 1100 ℃. The SiC addition helped to suppress the particle growth for $Y_3Fe_5O_{12}$ at the calcination temperature. The heat generation ability was improved by the addition of the SiC powder, and the maximum value of 0.93 $W \cdot g^{-1}$ was obtained for the $n = 0.3$ sample calcined at 1250 ℃. The heat generation ability and the hysteresis loss value were proportional to the cube of the magnetic field (H^3). The heat generation ability ($W \cdot g^{-1}$) of the $Y_3Fe_5O_{12}$–0.3SiC sample calcined at 1250 ℃ could be expressed by the equation $4.5 \times 10^{-4} \cdot f \cdot H^3$ using the frequency f (kHz) and the magnetic field H ($kA \cdot m^{-1}$).

Keywords: magnetic materials; composite material; $Y_3Fe_5O_{12}$; SiC; heat generation ability; AC magnetic field

1 Introduction

The heat generation ability in an AC magnetic field for magnetic materials has been studied for the local treatment of cancerous tissues [1–7]. Materials of the needle type and powder type have been studied for this purpose. For the needle type metal materials, they are directly inserted from the surface into the tissues as in the case of cervical cancer and heated by an eddy loss in an AC magnetic field [8–10].

In the case of the powder type materials, a nano-sized superparamagnetic magnetite (Fe_3O_4) prepared by the chemical synthesis method has been investigated as the candidate material for this type of therapy [11–14]. We have searched for new magnetic materials having a high heat generation ability in an AC magnetic field and a high stability in the human body, and found that $Y_3Fe_5O_{12}$ has the best heat ability among the reported materials [15–22]. For the nano-sized superparamagnetic $Y_3Fe_5O_{12}$ material, bead milling was very effective for obtaining the high heat generation ability [16–20]. The heat generation ability of $Y_3Fe_5O_{12}$ was higher than that of the candidate Fe_3O_4 material for such an application. The heat generation mechanism was mainly ascribed to the Néel relaxation of the superparamagnetic materials [21,22]. The high heat

* Corresponding author.
E-mail: aono.hiromichi.mf@ehime-u.ac.jp

generation ability in an AC magnetic field was also obtained for the ferrimagnetic $Y_3Fe_5O_{12}$ powder material prepared by a reverse coprecipitation method [23]. For the normal coprecipitation method, the pH value gradually increases, because an alkali solution is added to the mixed metal solution. For this method, the final pH value influences the phase formation and particle size of the precursor [24]. In the case of the reverse coprecipitation method, the mixed metal solution was directly added to an alkaline solution to maintain a high pH in order to obtain the homogeneous metal hydroxide [25]. The heat generation for the ferrimagnetic materials is due to the hysteresis loss for the *B*–*H* magnetic property. In this $Y_3Fe_5O_{12}$, the maximum heat generation ability in the AC magnetic field was obtained by calcination at 1100 ℃ for the sample having a ca. 1.0 μm particle size. However, the particle growth due to calcination at a higher temperature caused a decrease in the heat generation ability. The intentional addition of a second phase would be an effective way to suppress the decrease in the heat generation ability with the particle growth during the calcination treatment. We considered that the SiC powder having a high melting point acts as a material that suppresses the particle growth. In addition, it is possible to only evaluate in detail the effects of the particle suppression, because the SiC itself does not affect for the heat generation ability being the nonmagnetic material.

In this study, the SiC powder was selected for the second phase and the ferrimagnetic $Y_3Fe_5O_{12}$–*n*SiC system prepared by the reverse coprecipitation method was investigated for its heat generation ability in an AC magnetic field.

2 Experimental

2. 1 Sample preparation and characterization

$Y_3Fe_5O_{12}$ was prepared by a reverse coprecipitation method [25]. For the preparation of the precursor, stoichiometric materials of $Y(NO_3)_3{\cdot}6H_2O$ and $Fe(NO_3)_3{\cdot}9H_2O$ as $Y_3Fe_5O_{12}$ (0.03 mol) were dissolved in pure water (200 mL) to form the mixed solution. Stoichiometric SiC powder (Kojundo Chemical Laboratory Co., Ltd., 99%) for the $Y_3Fe_5O_{12}$–*n*SiC system was suspended in this mixed solution. An NaOH solution (6 mol/L, 140 mL) was placed in a hot water bath at 100 ℃. The mixed suspension of the nitrates and the SiC powder was then directly added at the rate of 1.5 mL/min to the NaOH solution with stirring, and held at 90–100 ℃ for 1 h. The final pH value of the solution was higher than 13. The precipitate was filtered and washed with distilled or deionized water until the pH of the wash water dropped below 9. After the powder (the precursor) was dried at 70 ℃, it was then calcined at various temperatures in the range of 900–1300 ℃ for 1 h in ambient air.

The X-ray diffraction (XRD) patterns of the calcined powder were recorded using a Rigaku Rint 2000 diffractometer with Cu Kα radiation (scanning rate = 2 (°)/min at 40 kV and 20 mA). The specific surface area was measured by the one-point Brunauer–Emmett–Teller (BET) method and then the particle size was calculated by assuming a spherical particle. The estimated particle size using this method was ca. 0.9 μm for the mixed SiC powder.

2. 2 Measurement of heat generation ability

Figure 1 shows the apparatus for measuring the heat generation ability of the sample powder in the AC magnetic field. The $Y_3Fe_5O_{12}$–*n*SiC sample powder (2.0 g) in 10 mL of water (16.7 wt% ferrite concentration) was placed in a glass case (Pyrex: 20 mm∅, 45 mm) and the AC magnetic field (370 kHz and 1.77 $kA{\cdot}m^{-1}$) was applied to the sample using an external coil. The temperature of the sample was measured using a radiation thermometer (TP-L0225EN, Chino Co.). The temperature measurement was started after maintaining the temperature at 25 ℃ in ambient air for several hours. Air was bubbled into the glass case for stirring the sample powder in the water. The heat generation ability ($W{\cdot}g^{-1}$) was calculated based on the temperature enhancement ratio dT/dt ($K{\cdot}s^{-1}$) during the initial 5 min of the temperature measurement using the

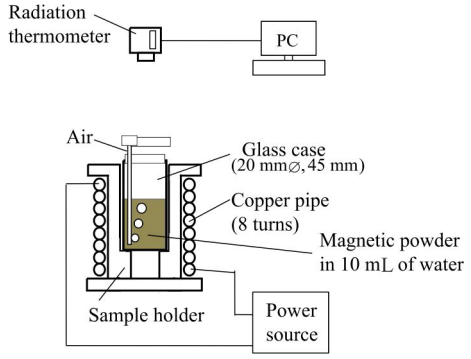

Fig. 1 Apparatus for measurement of the heat generation ability of the ferrite powder in an AC magnetic field.

following equation:

$$\text{Heat generation ability} = C \cdot (\mathrm{d}T/\mathrm{d}t) \cdot M^{-1} \quad (1)$$

where M and C are the sample weight (g) and the estimated total heat capacity ($J \cdot K^{-1}$) of 10 mL of water and the glass case, respectively. The average value for the measurement of three samples or more was used for this calculation.

2. 3 Measurement of hysteresis loss

The hysteresis loss in the AC magnetic field (370 kHz, 0.1–1.77 $kA \cdot m^{-1}$) was obtained using a *B–H* analyzer (Iwatsu Electric Co., Ltd., SY-8258). For this measurement, ring type samples (about 24 mm outside diameter, about 13 mm inside diameter, about 5 mm height) were prepared using a mixture of the ferrite powder and epoxy resin adhesive (4:1 weight ratio, 80 wt% ferrite concentration).

3 Results and discussion

3. 1 Characterization of sample powder

The precursor for $Y_3Fe_5O_{12}$ obtained using the reverse coprecipitation method mainly consisted of mixed metal hydroxides. For the thermogravimetric (TG) analysis, the weight of the precursor gradually decreased with an increase in the temperature and showed a constant value for forming the metal oxide at around 820 ℃. Figure 2 shows the XRD results for the $Y_3Fe_5O_{12}$–*n*SiC ((a) $n = 0$, (b) $n = 0.3$, and (c) $n = 1.0$) calcined at various temperatures. In the case of (a) $n = 0$, the main cubic $Y_3Fe_5O_{12}$ phase with a low intensity of the orthorhombic $YFeO_3$ phase was detected for the sample calcined at 1100 ℃. The $YFeO_3$ phase almost disappeared by calcination at 1150 ℃ or higher. The peak intensity of $YFeO_3$ was increased for the SiC added (Fig. 2(b), $n = 0.3$). For the (c) $n = 1.0$ sample, the $YFeO_3$ phase was mainly formed with the $Y_3Fe_5O_{12}$ along with the added SiC phase for the sample calcined at 900 ℃. The peak intensity of the $YFeO_3$ and added SiC phases was reduced with an increase in the calcination temperature. The formation of the silicates and peak shift (change in the lattice parameters) for the $Y_3Fe_5O_{12}$ were not detected for the $n = 1.0$ sample calcined at a high temperature. The SiC phase would decompose into an amorphous oxide phase at around 1000 ℃. However, the $YFeO_3$ phase remained even by calcination at 1250 ℃. The formed SiO_2 amorphous phase at the grain boundary would act to suppress the solid reaction to form the $Y_3Fe_5O_{12}$ single phase.

Figure 3 plots the particle diameters of the calcined samples for the $Y_3Fe_5O_{12}$–*n*SiC system. The particle diameter was estimated from the surface area of the powder samples. These values are listed in Table 1. The particle diameter increased with the calcination temperature for all the evaluated samples. For the non-SiC added sample ($n = 0$), the particles grew to several micrometer for the samples calcined at 1150 ℃ and higher. The particle growth seems to occur when the $YFeO_3$ second phase disappeared in the mixed phase [23]. For the SiC added samples, the particle growth was suppressed even for the samples calcined at 1200 ℃ and higher. Figure 4 shows the scanning electron microscopy (SEM) images of the samples calcined at various temperatures for the $Y_3Fe_5O_{12}$–*n*SiC system. The samples having similar particle size were selected for comparison of their particle shape. For the non-SiC added sample ($n = 0$) calcined at 1100 ℃ (Fig. 4(a)), relatively large particles having a slim elliptic shape were observed in the photo. For the SiC added samples, the particle growth did not progress

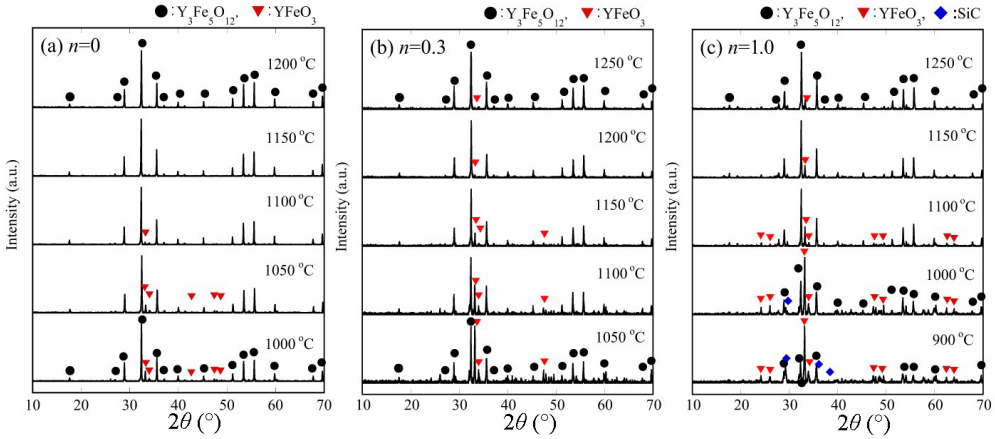

Fig. 2 XRD results of the calcined precursor for the $Y_3Fe_5O_{12}$–*n*SiC system synthesized by the reverse coprecipitation method: (a) $n = 0$, (b) $n = 0.3$, and (c) $n = 1.0$. The calcination temperature is shown in the figure.

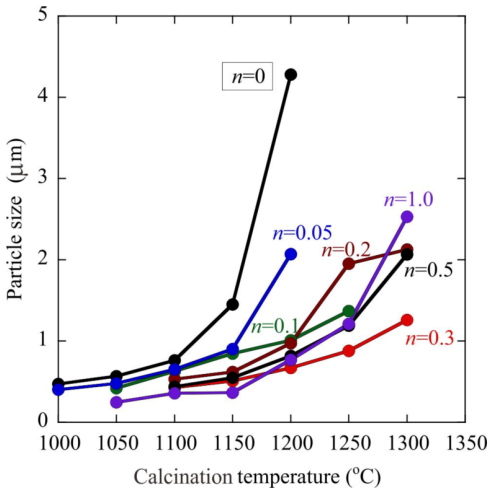

Fig. 3 Relationship between the calcination temperature and particle size for the $Y_3Fe_5O_{12}$–*n*SiC system.

even at higher temperatures, but formed homogeneous round-shaped particles for the samples of $n = 0.3$ at 1250 ℃ (Fig. 4(b)) and $n = 1.0$ at 1300 ℃ (Fig. 4(c)).

3. 2 Heat generation ability

Figure 5 shows the relationship between the sintering temperature and the heat generation ability in an AC magnetic field (370 kHz, 1.77 kA·m^{-1}). For the non-SiC added sample ($n = 0$), the heat generation ability increased with the calcination temperature and the maximum value of ca. 0.46 W·g^{-1} was obtained for the sample calcined at 1100 ℃. The heat generation ability decreased with the calcination temperature above 1150 ℃ for $n = 0$. Although the tendency for the heat generation ability was similar with $n = 0$ for the SiC added samples, the calcination temperature for the maximum heat generation ability shifted to 1200–1300 ℃. The maximum heat generation value was increased by the SiC addition. Figure 6 plots the relationship between the *n* value and the maximum heat generation ability in each *n* sample in Fig. 5. In the case of the SiC added samples, the calcination temperature for the maximum heat generation ability was increased and showed a higher ability compared to that of the $n = 0$ sample. The maximum value for $n = 0.3$ was 0.93 W·g^{-1} which was two times higher than that of the $n = 0$ sample. The excessive SiC addition reduced the heat generation because of its nonmagnetic property. This improvement in the heat generation ability would be ascribed to the increase in the calcination temperature to form homogeneous and suitable $Y_3Fe_5O_{12}$ particles for the heat generation. Figure 7 shows the relationship between the particle diameter

Table 1 Particle size (μm) and surface area (m^2·g^{-1}, in the brackets) for the calcined samples of the $Y_3Fe_5O_{12}$–*n*SiC system

Calcination temperature	$n = 0$	$n = 0.05$	$n = 0.1$	$n = 0.2$	$n = 0.3$	$n = 0.5$	$n = 1.0$
1000 ℃	0.473 (2.45)	0.403 (2.88)	—	—	—	—	—
1050 ℃	0.569 (2.04)	0.478 (2.43)	0.422 (2.75)	—	—	—	0.248 (4.78)
1100 ℃	0.763 (1.52)	0.652 (1.78)	0.629 (1.84)	0.532 (2.18)	0.430 (2.70)	0.440 (2.64)	0.359 (3.23)
1150 ℃	1.45 (0.800)	0.901 (1.29)	0.847 (1.37)	0.620 (1.87)	0.510 (2.27)	0.549 (2.11)	0.366 (3.17)
1200 ℃	4.28 (0.271)	2.07 (0.560)	1.01 (1.15)	0.973 (1.19)	0.670 (1.73)	0.817 (1.42)	0.770 (1.51)
1250 ℃	—	—	1.37 (0.847)	1.95 (0.595)	0.880 (1.32)	1.19 (0.975)	1.21 (0.959)
1300 ℃	—	—	—	2.13 (0.545)	1.26 (0.920)	2.07 (0.560)	2.53 (0.458)

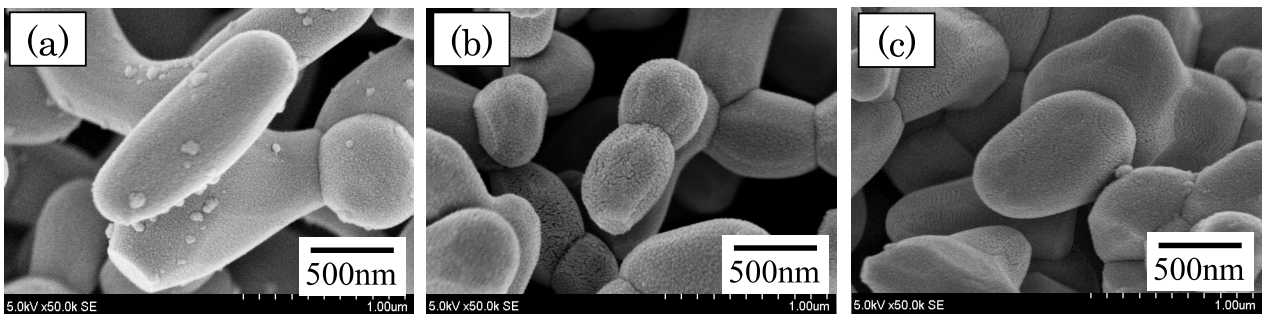

Fig. 4 Field emission SEM observations of the surface for (a) $Y_3Fe_5O_{12}$ calcined at 1100 ℃, (b) $Y_3Fe_5O_{12}$–0.3SiC calcined at 1250 ℃, and (c) $Y_3Fe_5O_{12}$–1.0SiC calcined at 1300 ℃.

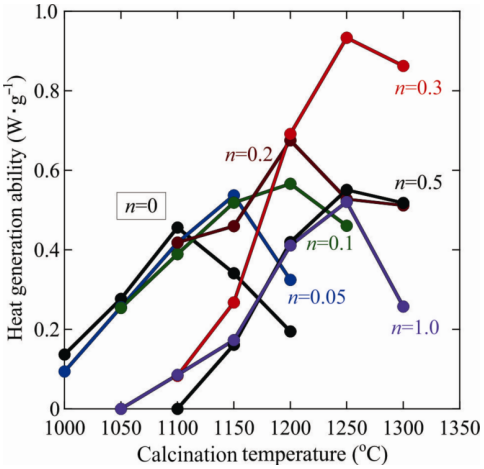

Fig. 5 Relationship between the calcination temperature and the heat generation ability in an AC magnetic field (370 kHz, 1.77 kA·m^{-1}) for the $Y_3Fe_5O_{12}$–nSiC system.

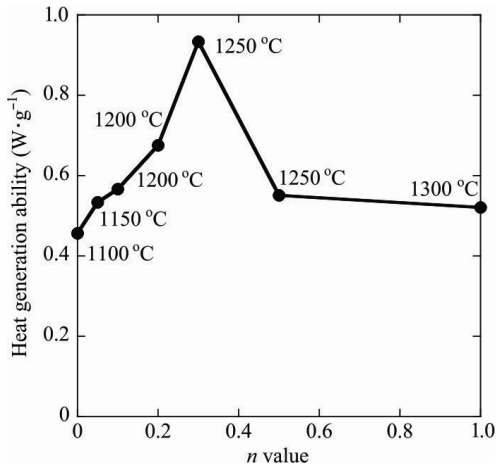

Fig. 6 Relationship between the n value and the maximum heat generation ability for each n sample of the $Y_3Fe_5O_{12}$–nSiC system. The calcination temperature is shown in the figure.

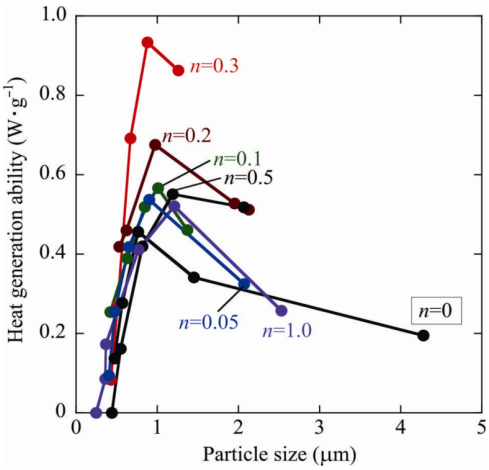

Fig. 7 Relationship between the particle diameter and the heat generation ability in an AC magnetic field (370 kHz, 1.77 kA·m^{-1}) for the $Y_3Fe_5O_{12}$–nSiC system.

and the heat generation ability in an AC magnetic field (370 kHz, 1.77 kA·m^{-1}). The maximum heat generation ability was obtained for the sample having an approximate 1.0 μm particle diameter. The heat generation ability decreased with the further particle growth.

Figure 8 shows the relationship between the cube of the magnetic field (H^3) and heat generation ability for the $n = 0.3$ samples calcined at 1200 ℃ and 1250 ℃. The hysteresis loss values for the B–H analysis are also plotted in this figure. The heat generation ability and the hysteresis loss value were proportional to the cube of the magnetic field (H^3) for all the examined samples. The heat generation ability and the hysteresis value closely agreed for the sample calcined at 1200 ℃. However, the hysteresis loss showed a higher value compared to the heat generation ability for the sample calcined at 1250 ℃. In our previous paper, the high concentration of ferrite powder was found to influence the convergence of the magnetic field for the samples having a large particle size, because the concentration of the ferrite powder (80 wt%) in the hysteresis measurement was greater than that (16.7 wt%) in the measurement of the heat generation ability [23]. The heat generation ability was also proportional to the frequency of the AC magnetic field. Based on these results, the heat generation ability is expressed as

$$\text{Heat generation ability (W·g}^{-1}) = k \cdot f \cdot H^3 \quad (2)$$

where k, f, and H are a constant value, frequency (kHz), and the magnetic field (kA·m^{-1}), respectively. The

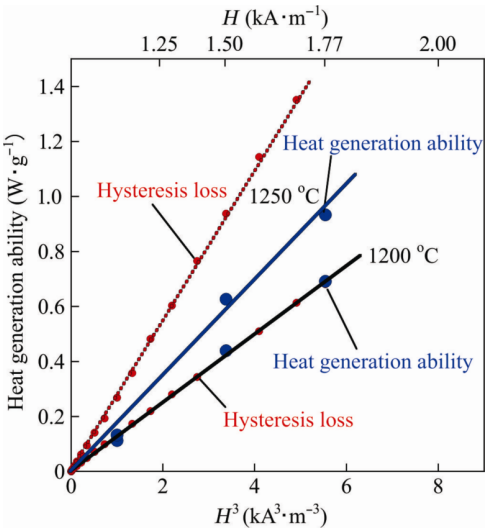

Fig. 8 Relationship between the cube of the magnetic field (H^3) and heat generation ability in an AC magnetic field (370 kHz) for the $n = 0.3$ samples calcined at 1200 ℃ and 1250 ℃. The hysteresis value using the B–H analysis is also plotted in the figure.

estimated k value in Eq. (2) using the heat generation ability was 3.4×10^{-4} and 4.5×10^{-4} for the total loss of the samples calcined at 1200 ℃ and 1250 ℃, respectively. The heat generation ability ($W\cdot g^{-1}$) of these ferrite materials in an AC magnetic field knowing the arbitrary frequency f (kHz) and the magnetic field H ($kA\cdot m^{-1}$) can be easily estimated using Eq. (2).

Figure 9 plots the heat generation ability and the hysteresis loss for the samples of the $Y_3Fe_5O_{12}$–nSiC ($n=0$, 0.3, and 1.0) system calcined at various temperatures. The heat generation ability and the hysteresis value closely agreed for the samples calcined at the lower temperatures for each n sample. As shown in Fig. 8, the hysteresis loss value showed a higher value compared to the heat generation ability for the samples calcined at higher temperature. These behaviors would be due to the influence of the ferrite concentration for the samples having a large particle size.

In our previous study, it was reported that $Y_3Fe_5O_{12}$ is the best material having the heat generation ability of $2.2\times10^{-4}\cdot f\cdot H^3$ involving the arbitrary frequency f (kHz) and the magnetic field H ($kA\cdot m^{-1}$) [23]. The heat generation was strongly improved by the SiC addition to the $Y_3Fe_5O_{12}$ and the maximum value was $4.5\times10^{-4}\cdot f\cdot H^3$ for the $Y_3Fe_5O_{12}$–0.3SiC sample calcined at 1250 ℃.

4 Conclusions

The material having a high heat generation ability was obtained for the $Y_3Fe_5O_{12}$–nSiC system. The SiC addition depressed the particle growth of the $Y_3Fe_5O_{12}$. The maximum heat generation ability was obtained for $n=0.3$ by calcination at 1250 ℃. This improvement in the heat generation ability would be ascribed to the increase in the calcination temperature to form homogeneous and suitable $Y_3Fe_5O_{12}$ particles for the heat generation. The heat generation ability ($W\cdot g^{-1}$) in an AC magnetic field could be estimated using the equation $4.5\times10^{-4}\cdot f\cdot H^3$ relating the arbitrary frequency f (kHz) and the magnetic field H ($kA\cdot m^{-1}$). This value is about two times higher than that of $Y_3Fe_5O_{12}$ ($n=0$).

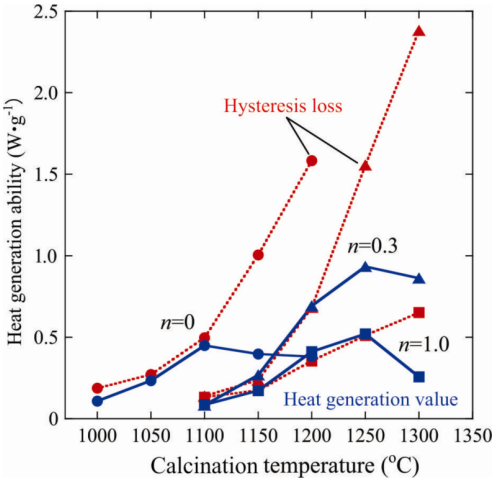

Fig. 9 Relationship between the calcination temperature and heat generation ability for the samples of the $Y_3Fe_5O_{12}$–nSiC ($n=0$, 0.3, and 1.0) system. The hysteresis value is also plotted in the figure.

References

[1] Moroz P, Jones SK, Gray BN. Magnetically mediated hyperthermia: Current status and future directions. *Int J Hyperther* 2002, **18**: 267–284.

[2] Johannsen M, Gneveckow U, Thiesen B, *et al*. Thermotherapy of prostate cancer using magnetic nanoparticles: Feasibility, imaging, and three-dimensional temperature distribution. *Eur Urol* 2007, **52**: 1653–1662.

[3] Jordan A, Scholz R, Maier-Hauff K, *et al*. The effect of thermotherapy using magnetic nanoparticles on rat malignant glioma. *J Neuro-Oncol* 2006, **78**: 7–14.

[4] Maier-Hauff K, Rothe R, Scholz R, *et al*. Intracranial thermotherapy using magnetic nanoparticles combined with external beam radiotherapy: Results of a feasibility study on patients with glioblastoma multiforme. *J Neuro-Oncol* 2007, **81**: 53–60.

[5] Yoshida M, Watanabe Y, Sato M, *et al*. Feasibility of chemohyperthermia with docetaxel-embedded magnetoliposomes as minimally invasive local treatment for cancer. *Int J Cancer* 2010, **126**: 1955–1965.

[6] Lee J-H, Jang J-t, Choi J-s, *et al*. Exchange-coupled magnetic nanoparticles for efficient heat induction. *Nat Nanotechnol* 2011, **6**: 418–422.

[7] Kumar CSSR, Mohammad F. Magnetic nanomaterials for hyperthermia-based therapy and controlled drug delivery. *Adv Drug Deliver Rev* 2011, **63**: 789–808.

[8] Aono H, Naohara T, Maehara T, *et al*. Heat generation ability in AC magnetic field and their computer simulation for Ti tube filled with ferrite powder. *J Magn Magn Mater* 2011, **323**: 88–93.

[9] Naohara T, Aono H, Maehara T, *et al*. Heat generation and transfer behaviors of Ti-coated carbon steel rod adaptable for ablation therapy of oral cancer. *J Funct Biomater* 2013, **4**: 27–37.

[10] Naohara T, Aono H, Hirazawa H, *et al*. Heat generation ability in AC magnetic field of needle-type Ti-coated mild steel for ablation cancer therapy. *COMPEL—The International Journal for Computation and Mathematics in Electrical and Electronic Engineering* 2011, **30**: 1582–1588.

[11] Shinkai M, Yanase M, Suzuki M, *et al*. Intracellular hyperthermia for cancer using magnetite cationic liposomes. *J Magn Magn Mater* 1999, **194**: 176–184.
[12] Ma M, Wu Y, Zhou J, *et al*. Size dependence of specific power absorption of Fe_3O_4 particles in AC magnetic field. *J Magn Magn Mater* 2004, **268**: 33–39.
[13] Aono H, Hirazawa H, Naohara T, *et al*. Synthesis of fine magnetite powder using reverse coprecipitation method and its heating properties by applying AC magnetic field. *Mater Res Bull* 2005, **40**: 1126–1135.
[14] Aono H, Nagamachi T, Naohara T, *et al*. Synthesis conditions of nano-sized magnetite powder using reverse coprecipitation method for thermal coagulation therapy. *J Ceram Soc Jpn* 2016, **124**: 23–28.
[15] Aono H, Moritani K, Naohara T, *et al*. New heat generation material in AC magnetic field for $Y_3Fe_5O_{12}$-based powder material synthesized by reverse coprecipication method. *Mater Lett* 2011, **65**: 1454–1456.
[16] Nishimori T, Naohara T, Maehara T, *et al*. Heat generation properties in AC magnetic field for ferrimagnetic $R_3Fe_5O_{12}$ (R = Y, Sm, Gd, Dy, Ho, Er) powder materials synthesized by reverse coprecipitation method. *J Iron and Steel Res, International, Suppl 1* 2012, **19**: 600–603.
[17] Aono H, Ebara H, Senba R, *et al*. High heat generation ability in AC magnetic field for $Y_3Fe_5O_{12}$ powder prepared using bead milling. *J Am Ceram Soc* 2011, **94**: 4116–4119.
[18] Aono H, Ebara H, Senba R, *et al*. High heat generation ability in AC magnetic field for nano-sized magnetic $Y_3Fe_5O_{12}$ powder prepared by bead milling. *J Magn Magn Mater* 2012, **324**: 1985–1991.
[19] Aono H. Development of nano-sized superparamagnetic ferrites having heat generation ability in an AC magnetic field for thermal coagulation therapy. *J Ceram Soc Jpn* 2014, **122**: 237–243.
[20] Aono H, Senba R, Nishimori T, *et al*. Preparation of $Y_3Fe_5O_{12}$ microsphere using bead-milled nanosize powder for embolization therapy application. *J Am Ceram Soc* 2013, **96**: 3483–3488.
[21] Nishimori T, Akiyama Y, Naohara T, *et al*. Effect of particle growth on heat generation ability in AC magnetic field for nano-sized magnetic $Y_3Fe_5O_{12}$ powder prepared by bead milling. *J Ceram Soc Jpn* 2013, **121**: 13–16.
[22] Nishimori T, Akiyama A, Naohara T, *et al*. Depression of particle growth with calcination at low temperature and their heat generation property in AC magnetic field for the nano-sized magnetic $Y_3Fe_5O_{12}$–$n$$SmFeO_3$ powders prepared by bead-millidng. *J Ceram Soc Jpn* 2014, **122**: 35–39.
[23] Aono H, Yamano Y, Nishimori T, *et al*. Heat generation properties in AC magnetic field for $Y_3Fe_5O_{12}$ powder material synthesized by a reverse coprecipitation method. *Ceram Int* 2015, **41**: 8461–8467.
[24] Praveena K, Sadhana K, Srinath S, *et al.* Effect of pH on structural and magnetic properties of nanocrystalline $Y_3Fe_5O_{12}$ by aqueous co-precipitation method. *Mater Res Innov* 2014, **18**: 69–75.
[25] Teraoka Y, Nanri S, Moriguchi I, *et al*. Synthesis of manganite perovskites by reverse homogeneous precipitation method in the presence of alkylammonium cations. *Chemistry Letters* 2000, **29**: 1202–1203.